Combination of the many-body perturbation theory with the configuration-interaction method

V. A. Dzuba*
School of Physics, University of New South Wales, Sydney, 2052, Australia

V. V. Flambaum†
Institute for Theoretical Atomic and Molecular Physics, Harvard-Smithsonian Center for Astrophysics and Harvard University, 60 Garden Street, Cambridge, Massachusetts 02138

M. G. Kozlov‡
Petersburg Nuclear Physics Institute, Gatchina, 188350, Russia
(Received 6 March 1996; revised manuscript received 25 July 1996)

An *ab initio* method for high accuracy calculations for atoms with more than one valence electron is described. The effective Hamiltonian for the valence electrons is formed using many-body perturbation theory for the interaction of the valence electrons with the core. The configuration-interaction method is then used to find the energy levels of the atom. An application of this to thallium shows that the method gives an accuracy of about 0.5% for the ionization potential and a few tenths of a percent for the first few energy intervals. [S1050-2947(96)08911-1]

PACS number(s): 31.15.Ar, 31.15.Md

I. INTRODUCTION

The development of new methods for high-precision atomic calculations is necessary not only for atomic physics itself, but also for applying atomic physics to the investigation of the fundamental interactions (see, e.g., [1–4]). At present, 1% accuracy has been reached in several measurements of parity nonconservation (PNC) in cesium [5], lead [6], thallium [7], and bismuth [8]. But until now the same theoretical accuracy has only been reached for cesium [9,10] and francium [11]. All these calculations were made within many-body perturbation theory (MBPT) [12–15]. In Refs. [9,11,14,15] the dominant series of higher-order diagrams were found and summed up in all orders. As the most important higher-order diagrams describe the effect of the screening of the Coulomb interaction by the core electrons, the method developed can be called ''perturbation theory in the screened Coulomb interaction'' (PTSCI). This method produces excellent results for alkali-metal atoms, which have one external electron above closed shells. The accuracy is about 0.1% for energy levels [11,14] and about 1% for hyperfine structure intervals and transition amplitudes [9,11,15]. Formally, atoms such as thallium can also be considered as having one external electron above closed subshells. However, the application of PTSCI to Tl gives only 1.5% accuracy for the ionization potential [16]. The reason is obvious: the interaction between the $6s$ and $6p$ electrons in Tl is too strong to be treated accurately by means of perturbation theory even though some types of diagrams are included in all orders.

There is an alternative coupled-cluster (CC) approach (see, e.g., [12]) in which some other series of higher-order diagrams are summed up in all orders thus taking into account pair correlations. Some relativistic CC calculations for many-electron atoms were performed in [17,18]. For alkali-metal atoms a similar accuracy as for PTSCI was achieved. However, for atoms with more complicated electron structures the typical accuracy was about 1% [18]. The most obvious shortcoming of the method is the neglect of three-particle correlations. Also, the CC method treats the valence-valence and core-valence correlations at the same level of approximation. It is clear, however, that the former correlations are much stronger than the latter.

On the other hand there are methods which treat many-body effects in an accurate way, at least for valence electrons. These are the well-known configuration-interaction (CI) and multiconfiguration Hartree-Fock (MCHF) methods (see, e.g., [19]). CI and MCHF methods have been widely used by a number of authors for accurate calculations for many-electron atoms (see, e.g., [20]). Recently, the CI method was used for calculations of PNC effects in such complicated atoms as dysprosium [21], ytterbium [22], and bismuth [23]. In principle, the accuracy of CI is limited only by the incompleteness of the set of configurations used. For a many-electron atom the number of possible configurations is so large that one has to select only a small fraction of them. This is usually done by neglecting core excitations or only including a very limited number of them. This in turn significantly limits the accuracy of the method.

It is important to stress here that the accuracy of the MBPT and the CI methods is restricted in different sectors of the many-body problem. MBPT is not accurate in describing valence-valence interactions, while CI fails to fully account for the core-valence and core-core correlations. For this reason it is natural to combine the two methods in an attempt to reach high accuracy for atoms with more than one valence electron. In the present paper we construct a combination of the two methods in the following way. All atomic electrons

*Electronic address: dzuba@newt.phys.unsw.edu.au
URL: http://www.phys.unsw.edu.au/~ dzuba/dzuba.html
†Electronic address: flambaum@cfaitamp3.harvard.edu
On leave from School of Physics, University of New South Wales, Sydney, 2052, Australia. Electronic address: v.flambaum@unsw.edu.au
‡Electronic address: kozlov@lnpi.spb.su

are divided into the valence electrons and the core electrons. The MBPT is used to construct an effective CI Hamiltonian in the model space of the valence electrons. This Hamiltonian includes additional terms to the ordinary CI method, which account for core-core and core-valence correlations. The CI method is used then to find atomic energy levels and wave functions.

In this paper we restrict ourselves to the calculation of energy levels, in particular those of Tl, Tl^+, and Tl^{2+}, but the method can be extended to calculate transition amplitudes and expectation values as well. Our final goal is to calculate the parity nonconserving $E1$ amplitudes for those atoms for which precise PNC measurements are underway, i.e., thallium, lead, and bismuth. A brief report of this work was published in [24].

II. METHOD

A. Configuration and perturbation subspaces

Let us divide the Hilbert space of the many-electron problem into two subspaces. The first subspace (P) corresponds to the frozen-core approximation. The second subspace (Q) includes all core excitations and is complementary to the first one.

It is natural to assume that the projections of the wave functions of the lower energy levels of the atom onto the subspace Q will be small. This allows us to take into account the subspace Q by means of MBPT. On the other hand, perturbation theory is not effective in the subspace P and so the CI method is preferable here.

Such a decomposition of the Hilbert space depends on the definition of the core. First, one should choose the number of electrons to be included in the core ($N_{\rm core}$). For example, the thallium atom can be treated as either a one-electron atom ($N_{\rm core}=80$) or as a three-electron atom ($N_{\rm core}=78$). For the convergence of MBPT it is important that the core and valence electrons be well separated in space and on the energy scale. In many cases that can be achieved by attributing to the core all of the subshells of a particular shell.

Second, it is necessary to specify the one-particle wave functions for the core electrons. Because we are going to use MBPT, these functions should be the eigenfunctions of some one-particle Hamiltonian:

$$h_0\phi_i=\epsilon_i\phi_i\,. \tag{1}$$

The choice of h_0 is discussed in Sec. III.

We can use Slater determinants $|I\rangle$ of the functions ϕ_i as a basis set in the many-electron space. It is easy to determine to which of the two subspaces any particular determinant $|I\rangle$ belongs. If all $N_{\rm core}$ lowest states are occupied, then $|I\rangle$ belongs to the subspace P, otherwise it belongs to the subspace Q.

Thus, we can write a projector to the subspace P as

$$\mathcal{P}=\sum_{I\in P}|I\rangle\langle I|, \tag{2}$$

and define a projector Q by the completeness condition

$$\mathcal{P}+Q=1. \tag{3}$$

B. Effective Hamiltonian for the CI problem

The subspace P is infinite-dimensional. Thus, it is impossible to find an exact solution of the Schrödinger equation in this subspace. However, if the number of the valence electrons is small enough (i.e., does not exceed three or four), it is possible to find a very good approximation with the help of the CI method. In this method a finite-dimensional model space $P^{\rm CI}\subset P$ is introduced by specifying the set of the allowed configurations for the valence electrons. The many-electron wave function is presented as a linear combination of Slater determinants from the model subspace,

$$\psi=\sum_{I\in P^{\rm CI}}C_I|I\rangle. \tag{4}$$

Variation of C_I leads to the matrix eigenvalue problem:

$$\sum_{J\in P^{\rm CI}}H_{IJ}C_J=EC_I\,, \tag{5}$$

which means that the energy matrix of the CI method can be obtained as a projection of the exact Hamiltonian $\mathcal{H}$ onto the model subspace:

$$\mathcal{H}^{\rm CI}=\mathcal{P}^{\rm CI}\mathcal{H}\mathcal{P}^{\rm CI}. \tag{6}$$

We will suppose that it is possible to choose $P^{\rm CI}$ so that the desired accuracy of the solution of the Schrödinger equation in the P subspace can be achieved. For this reason, below we will not distinguish between $P^{\rm CI}$ and P.

Let us write the operator $\mathcal{PHP}$ explicitly. Because the core in the subspace P is frozen, we can exclude core electrons from consideration by averaging the Hamiltonian over the single-determinant wave function of the core electrons. After that the operator $\mathcal{PHP}$ has the following form:

$$\mathcal{PHP}=E_{\rm core}+\sum_{i>N_{\rm core}}h_i^{\rm CI}+\sum_{j>i>N_{\rm core}}\frac{1}{r_{ij}}, \tag{7}$$

where $E_{\rm core}$ includes the kinetic energy of the core electrons and their Coulomb interaction with the nucleus and each other. The one-particle operator $h^{\rm CI}$ acts on the valence electrons and includes the kinetic term and the Coulomb interaction with the nucleus and with the core electrons. The last term in Eq. (7) accounts for the interaction of the valence electrons with each other. Atomic units are used throughout the paper, unless otherwise stated.

Operator (7) can be used in Eq. (5) instead of $\mathcal{H}$. In this case determinants $|I\rangle$ and $|J\rangle$ include only the valence electrons. This equation corresponds to the pure CI method in the frozen-core approximation.

To write the exact equivalent of the original Schrödinger equation in the subspace P let us make the P,Q decomposition of the Hamiltonian and the wave function of the many-body problem:

$$\mathcal{H}=\mathcal{PHP}+\mathcal{PHQ}+\mathcal{QHP}+\mathcal{QHQ}, \tag{8}$$

$$\Psi=P\Psi+Q\Psi\equiv\Phi+\chi. \tag{9}$$

The Schrödinger equation

$$\mathcal{H}\Psi = E\Psi \tag{10}$$

can be written as a system of equations for Φ and χ:

$$(\mathcal{PHP})\Phi + (\mathcal{PHQ})\chi = E\Phi \tag{11}$$

$$(\mathcal{QHQ})\chi + (\mathcal{QHP})\Phi = E\chi. \tag{12}$$

We can now define the Green's function in the subspace Q:

$$\mathcal{R}_Q(E) = (E - \mathcal{QHQ})^{-1}, \tag{13}$$

and then use Eq. (12) to exclude χ:

$$\chi = R_Q(E)(\mathcal{QHP})\Phi. \tag{14}$$

This gives us a Schrödinger-like equation in the subspace P, with an energy-dependent effective Hamiltonian:

$$(\mathcal{PHP} + \Sigma(E))\Phi = E\Phi, \tag{15}$$

$$\Sigma(E) = (\mathcal{PHQ})\mathcal{R}_Q(E)(\mathcal{QHP}). \tag{16}$$

By substituting (14) into (9) we can also rewrite the orthonormality conditions for the solutions of Eq. (10) in terms of the solutions of Eq. (15):

$$\langle\Phi_i|1 + (\mathcal{PHQ})R_Q(E_i)R_Q(E_k)(\mathcal{QHP})|\Phi_k\rangle = \delta_{ik}. \tag{17}$$

Equations (15)–(17) and (14) are the exact equivalent of Eq. (10). Because of the energy dependence of the operators Σ and $\mathcal{R}_Q$, these equations should be solved iteratively. If we are only interested in a few low-lying energy levels, then, in the first approximation, we can neglect this energy dependence and evaluate both operators for some energy $E_{\rm av} \simeq E_i \simeq E_k$. In this approximation Eq. (17) is expressed in terms of the derivative of the operator (16):

$$\langle\Phi_i|1 - \partial_E\Sigma(E)|\Phi_k\rangle_{E=E_{\rm av}} = \delta_{ik}. \tag{18}$$

Actually, for the proper choice of the P subspace, $\partial_E\Sigma(E)$ can be so small that the usual orthonormality condition can be applied. In this case, the standard CI procedures can be used to solve Eq. (15), provided that the operator $\Sigma(E_{\rm av})$ is calculated beforehand. The latter can be calculated with the help of MBPT, as described in some detail in the next section.

If the subspace P includes only one electron the operator $\mathcal{PHP}$ is reduced to the Dirac-Fock operator with the V^{N-1} potential and Σ is reduced to the single-particle self-energy operator. In this case Eqs. (15) and (18) define Bruckner orbitals and so the operator Σ can be considered as a direct generalization of the single-particle self-energy operator Σ to the case of several valence electrons.

III. MANY-BODY PERTURBATION THEORY FOR Σ

A. Perturbation expansion

In this section we are going to obtain a perturbation expansion for expression (16). The form of this expansion depends on the choice of the operator h_0 (1), which determines the starting approximation. The simplest form of the expansion corresponds to the $V^{N_{\rm core}}$ approximation, for which h_0 is the Dirac-Fock operator for the core. However, when the number of valence electrons is more than one this approximation is too crude to start with, as it corresponds to a multiply charged ion rather than a neutral atom. This means that some or all of the valence electrons should also be included in the self-consistent procedure. For the case of thallium it is better to use the V^{N-1} approximation (see, e.g., [25]). The Hartree-Fock procedure is done for the closed-shell ion Tl^+, and the basis set of excited states for the valence electrons is calculated in the field of the frozen Tl^+ core.

Let us define $N_{\rm DF}$ as the number of electrons included in the Hartree-Fock self-consistent procedure: $N_{\rm core} \leqslant N_{\rm DF} \leqslant N$, N being the total number of electrons in the atom. Now we can define h_0 as the corresponding Dirac-Fock operator:

$$h_0 \equiv h_{\rm DF} = c\boldsymbol{\alpha}\times\boldsymbol{p} + (\beta - 1)mc^2 - \frac{Z}{r} + V^{N_{\rm DF}}. \tag{19}$$

Let us introduce the creation (annihilation) operators $a_i^\dagger$ (a_i) for the functions (1):

$$h_{\rm DF}a_i^\dagger|0\rangle = \epsilon_i a_i^\dagger|0\rangle, \tag{20}$$

where ϵ_i is the Dirac-Fock energy of the orbital i. The corresponding Dirac-Fock operator in the many-electron space, $H_{\rm DF}$, can be written as

$$H_{\rm DF} = E_{\rm core} - \sum_{m=1}^{N_{\rm core}} \epsilon_m b_m^\dagger b_m + \sum_{i>N_{\rm core}} \epsilon_i a_i^\dagger a_i \equiv E_{\rm core} + \widetilde{H}_{\rm DF}, \tag{21}$$

where $b_m^\dagger = a_m$ and $b_m = a_m^\dagger$ are creation (annihilation) operators of holes in the core. The energy $E_{\rm core}$ in Eqs. (7) and (21) is defined as the matrix element of the exact Hamiltonian $\mathcal{H}$ with the core wave function:

$$E_{\rm core} = \langle\Psi_{\rm core}|\mathcal{H}|\Psi_{\rm core}\rangle, \tag{22}$$

$$\Psi_{\rm core} = a_1^\dagger a_2^\dagger \cdots a_{N_{\rm core}}^\dagger|0\rangle. \tag{23}$$

Note that the core wave function $\Psi_{\rm core}$ includes $N_{\rm core}$ electrons but is constructed from the solutions of Eq. (20) which corresponds to the self-consistent field of the $N_{\rm DF}$ electrons. That means that expression (22) differs from the Dirac-Fock energy of the ion with $N_{\rm core}$ electrons.

It follows from Eqs. (20), (21), and (23) that

$$\mathcal{PH}_{\rm DF}\mathcal{Q} = \mathcal{QH}_{\rm DF}\mathcal{P} = 0. \tag{24}$$

This allows us to rewrite Eq. (16) as

$$\begin{aligned}\Sigma(E) &= (\mathcal{P}(\mathcal{H} - \mathcal{H}_{\rm DF})\mathcal{Q})\mathcal{R}_Q(E)(\mathcal{Q}(\mathcal{H} - \mathcal{H}_{\rm DF})\mathcal{P}) \\ &= (\mathcal{P}(\mathcal{V} - \mathcal{V}^{N_{\rm DF}})\mathcal{Q})\mathcal{R}_Q(E)(\mathcal{Q}(\mathcal{V} - \mathcal{V}^{N_{\rm DF}})\mathcal{P}),\end{aligned} \tag{25}$$

where $\mathcal{V}$ is the operator of the two-electron Coulomb interaction and $\mathcal{V}^{N_{\rm DF}}$ is the operator of the interaction of the $N_{\rm DF}$ electrons with the Hartree-Fock field.

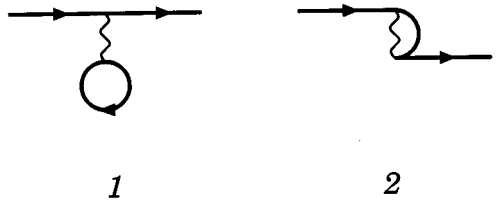

FIG. 1. First-order diagrams for the interaction of the valence electron with the core.

Expression (25) has the usual MBPT form. Now we can use the standard expansion for the operator $R_Q(E)$, treating $(\mathcal{V}-\mathcal{V}^{N_{\rm DF}})$ as a perturbation:

$$\begin{aligned}\mathcal{R}_Q(E) &\equiv \mathcal{Q}(E-\mathcal{H})^{-1}\mathcal{Q} \\ &= \mathcal{Q}(E-\mathcal{H}_{\rm DF})^{-1}\mathcal{Q}+\mathcal{Q}(E-\mathcal{H}_{\rm DF})^{-1}\mathcal{Q}(\mathcal{V} \\ &\quad -\mathcal{V}^{N_{\rm DF}})\mathcal{Q}(E-\mathcal{H}_{\rm DF})^{-1}\mathcal{Q}+\cdots . \end{aligned} \tag{26}$$

Substituting (26) into (25) and rewriting it in matrix form gives

$$\begin{aligned}\Sigma_{IJ} &= \sum_{M\in Q}\frac{U_{IM}U_{MJ}}{E-E_M}+\sum_{M,L\in Q}\frac{U_{IM}U_{ML}U_{LJ}}{(E-E_M)(E-E_L)}+\cdots \\ &\equiv \Sigma^{(2)}+\Sigma^{(3)}+\cdots , \end{aligned} \tag{27}$$

where $U=V-V^{N_{\rm DF}}$ is the residual interaction. The indices I and J enumerate determinants from the model space $P^{\rm CI}$, while indices M and L enumerate determinants from the space Q.

In the present paper we calculate Σ in the lowest- (second-) order of the perturbation expansion (for a discussion of higher-order correlations see below). Substituting $\Sigma^{(2)}$ into (15), we obtain the equation of the combined CI and MBPT method:

$$\sum_{J\in P^{\rm CI}}\left(H_{IJ}+\sum_{M\in Q}\frac{U_{IM}U_{MJ}}{E-E_M}\right)C_J=EC_I . \tag{28}$$

This equation differs from (5) by the $\Sigma^{(2)}$ term, which accounts for the correlations involving core electrons.

Note that the energy-dependent expression for Σ corresponds to Brillouin-Wigner perturbation theory [12]. There is an alternative Rayleigh-Schrödinger approach in which Σ is energy-independent. However, this approach has some disadvantages. The matrix of the eigenvalue problem (28) becomes nonsymmetric [26]. This is because of the difference in the energy denominators for the matrix elements $\Sigma^{(2)}_{IJ}$ and $\Sigma^{(2)}_{JI}$ (E_I-E_M and E_J-E_M, respectively). Furthermore, some of the denominators E_I-E_M could become small when the index I corresponds to a highly excited configuration.

Let us stress once more that in our approach only the excitations from the core are treated by means of MBPT. All valence-valence correlations are included directly into the matrix diagonalization. Thus, the Brillouin-Wigner formalism seems to be more appropriate in our case.

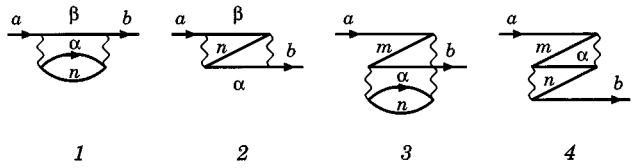

FIG. 2. Second-order diagrams for the self-energy of the valence electron.

B. Diagrammatic technique

1. Interaction with the core

In the zeroth order of MBPT the interaction of valence electrons with the core is described by the two diagrams (Fig. 1) where the sums for the internal lines run over the core. The interaction with the Hartree-Fock field corresponds to the same diagrams, but the sums run over the $N_{\rm DF}$ electrons. If $N_{\rm core}=N_{\rm DF}$, there is a complete cancellation of these two contributions. That means that all diagrams which have the blocks shown in Fig. 1 as one of their parts disappear. The same holds true for those blocks in which one of the external electron lines has been replaced by a hole line.

If $N_{\rm core}<N_{\rm DF}$, there will only be a partial cancellation of the core-valence interaction and the Hartree-Fock field. As a result, the diagrams containing blocks Fig. 1 survive, but the sums only run from $N_{\rm core}+1$ to $N_{\rm DF}$. Below we will call them subtraction diagrams [they appear due to the facts that the Hartree-Fock field is ''stronger'' than the core-valence interaction and that the Hartree-Fock field enters Eqs. (25) and (26) with a minus sign].

2. Pauli principle

All of the second-order diagrams which appear in the evaluation of $\Sigma^{(2)}$ are presented in Figs. 2–6. We omit the unlinked lines, which correspond to the states of the valence electrons that are not involved in the interaction. Thus, the diagrams shown are valid for any number of valence electrons, any atom and any particular choice of the core. However, the omitted lines do affect the value of the MBPT correction through the Pauli principle. Indeed, the states occupied by the valence electrons should be omitted from the summation over intermediate excited states. Implementing the Pauli principle ''by hand'' would make the diagrams determinant-dependent and would increase the amount of calculations dramatically. Fortunately, the Pauli principle

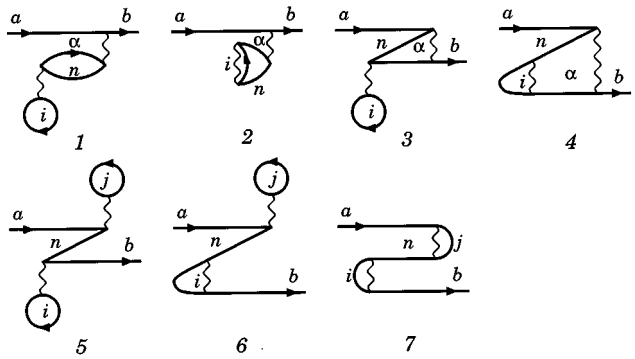

FIG. 3. Second-order subtraction diagrams for the self-energy.

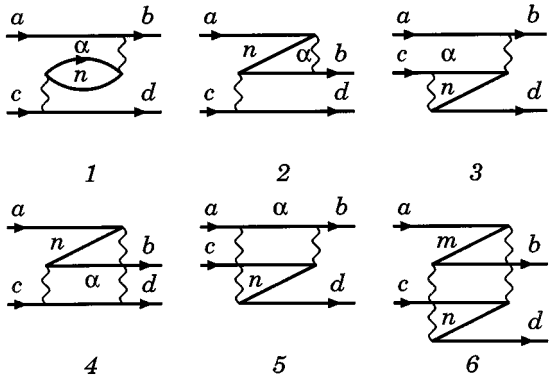

FIG. 4. Second-order diagrams for screening.

can be simply ignored due to the exact cancellation of the ''wrong'' terms in different diagrams. Note that this rule works in all orders of the perturbation theory. This makes the theory very similar to MBPT for atoms with one external electron ([14–16]). Two examples of the cancelation of the Pauli-forbidden contributions are shown in Fig. 7.

3. Diagrams with one external line

This is the so-called self-energy correction, which describes the correlation interaction of the valence electron with the core. The first four diagrams (Fig. 2) are the same as for ordinary MBPT (see, e.g., [16]).

Figure 3 shows the subtraction diagrams for the self-energy. Each asymmetrical diagram has a mirror image partner that is not shown explicitly. The subtraction diagrams can be quite large, and they significantly reduce the final value of the self-energy correction.

4. Diagrams with two external lines

The screening of the valence-valence interaction by the core electrons is described by the diagrams shown in Figs. 4 and 5. The resulting screening correction to the interaction between the valence electrons can be written in the form of an effective radial integral, as is usually done for the Coulomb integrals. However, one has to keep in mind the following specific features of the box diagrams in Figs. 4.4–4.6.

(1) The effective radial integrals for the box diagrams have lower symmetry than the Coulomb ones. In particular, interchanging the initial and final states in either the upper or lower lines changes the integral.

(2) For the box diagrams there is no correlation between the multipolarity and the parity of the transition. For example, the $A_{1/2} \rightarrow p_{1/2}$ transition can be either monopole or dipole. Indeed, the parity selection rule applies to the scalar sum of the angular momenta transferred through the Coulomb interaction, k_1+k_2, while the multipolarity of the effective radial integral corresponds to the vector sum $\boldsymbol{k}=\boldsymbol{k}_1+\boldsymbol{k}_2$.

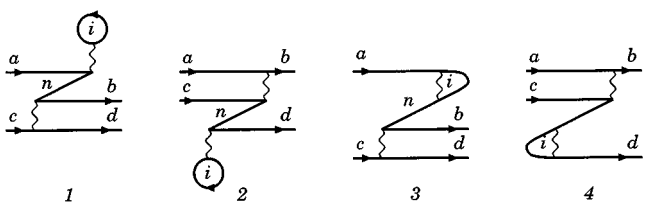

FIG. 5. Second-order subtraction diagrams for screening.

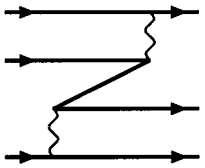

FIG. 6. Effective three-particle interaction between valence electrons.

These features increase the number of independent radial integrals by a factor of about four. On the other hand, the box diagrams appear to be much smaller than the diagrams in Figs. 4.1 – 4.3. For this reason it is possible to take them into account only for the few leading configurations. This allows one to store the effective radial integrals for other configurations in the same way as is done for the Coulomb integrals.

5. Diagrams with three external lines

The diagram shown in Fig. 6 represents an effective three-particle interaction in which three valence electrons interact with each other via the core. The diagrams of this type have only one internal summation and are much simpler than the one- and two-particle diagrams. However, the number of corresponding effective radial integrals is enormous. It is practically impossible to do large CI for the three-particle effective Hamiltonian. Fortunately, these diagrams can be made small by an appropriate choice of the atomic core. In particular, the core and valence states should have small overlap and be well separated energetically. These diagrams can then be either omitted altogether or included only within the leading configuration(s).

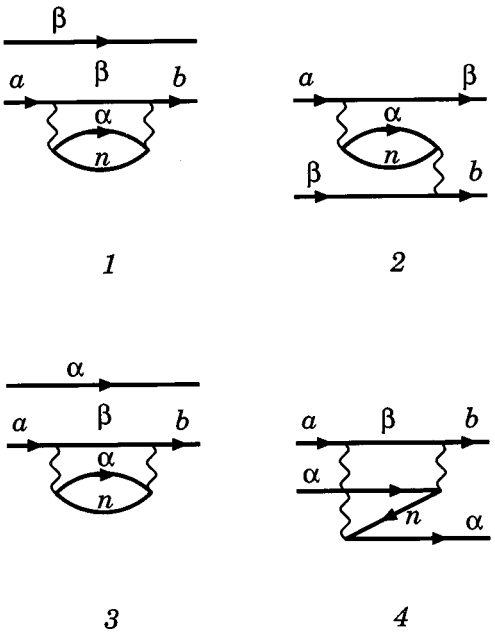

FIG. 7. Examples of diagrams which violate the Pauli principle. Diagrams 1 and 2 and 3 and 4 cancel each other exactly.

The diagrams of Figs. 2 – 6 give the complete set of the second-order contributions to Σ. Analytical expressions for these contributions are given in the Appendix. Apart from the small terms corresponding to the box diagrams of Figs. 4.4 – 4.6 and to the three-particle interaction (Fig. 6), they can be expressed in a form of the usual single-particle and two-particle radial integrals. This makes it easy to include them when the effective CI Hamiltonian is formed.

6. Energy denominators

Until now we have not considered the definition of the energy denominators in the expressions which correspond to the diagrams discussed above. The energy E which enters Eqs. (25) and (26) is the energy of the atom as a whole. According to Eq. (7) it can be written as the sum of the core and the valence parts: $E=E_{\rm core}+E_{\rm val}$. The core part then cancels in $E-\mathcal{H}_{\rm DF}$ [see Eq. (21)] and so Eq. (26) can be rewritten as:

$$\mathcal{R}_Q(E)=\mathcal{Q}(E_{\rm val}-\widetilde{\mathcal{H}}_{\rm DF})^{-1}\mathcal{Q}+\mathcal{Q}(E_{\rm val}-\widetilde{\mathcal{H}}_{\rm DF})^{-1}\mathcal{Q}(\mathcal{V}-\mathcal{V}^{N_{\rm DF}})\mathcal{Q}(E_{\rm val}-\widetilde{\mathcal{H}}_{\rm DF})^{-1}\mathcal{Q}+\cdots. \quad (29)$$

In this expression we still have the energy $E_{\rm val}$, which corresponds to all of the valence electrons. That means that when, for example, the diagrams from Fig. 2 are calculated, the energy that should be taken for the outer lines depends on the states of the other valence electrons. If there are three valence electrons and we are interested in the matrix element of Σ between the configurations (a,c,d) and (b,c,d) then the energy denominator for the diagram Fig. 2.1 is equal to $E_{\rm val}-\epsilon_c-\epsilon_d+\epsilon_n-\epsilon_\alpha-\epsilon_\beta$, while the usual diagrammatic rules give the denominator $\epsilon_a+\epsilon_n-\epsilon_\alpha-\epsilon_\beta$. These expressions differ by the substitution $E_{\rm val}-\epsilon_c-\epsilon_d\leftrightarrow\epsilon_a$. In other words, the energy denominators for the connected diagrams depend on the particular disconnected diagram of which they are part.

From the computational point of view it is impractical to calculate all of the disconnected diagrams and some simplification should be used. In the first approximation all connected diagrams can be evaluated at the energies which correspond to the main configuration(s). In the second approximation each diagram can be calculated together with its first derivative with respect to the energy. That does not require any additional integrals and can be done easily. Then, for each disconnected diagram a corresponding correction for the energy shift can be made. Note that the derivatives of the diagrams can also be used in Eq. (18). In principle, higher terms of the Taylor expansion can be taken into account as well.

7. Higher-order corrections

In the above treatment we restricted ourselves to the second order of the perturbation theory. In calculations for the alkali-metal atoms [9–11] the higher-order corrections were very important. In principle, it is also possible to include here the dominant higher-order corrections to the correlation potential and to the screening of the Coulomb interaction in the same way as was done in [9,11]. On the other hand, the combined method allows one to choose a core small enough to make higher-order corrections negligible. For example, the largest contributions to the core-valence interaction in cesium and francium comes from the $5p$ and $6p$ shells, respectively. Thus, if these shells are included in the valence space, MBPT corrections can be significantly reduced and the higher-order terms can be neglected. We also want to stress that there is no point in considering higher-order terms in the expansion (29) without an accurate treatment of the energy dependence of Σ in the second order, as discussed in the previous paragraph.

C. Orbital basis sets for CI and MBPT parts of the problem

In contrast to MBPT, where the basis set of the eigenvectors of the unperturbed Hamiltonian is used, CI can be done for any orthonormal set of orbitals. For the complete CI the number of configurations is proportional to $N_o^{N_e}$, where N_o is the number of orbitals and N_e is the number of valence electrons. Thus, it is very important for the effective application of the CI method to choose the orbital basis set which provides rapid convergence.

From this point of view, the Dirac-Fock orbitals are not the best choice. They are even less so, as the orbitals from the continuum should be included. In this paper we will use two very different basis sets, both providing reasonably fast convergence and giving very similar final results.

The first basis set is similar to the Dirac-Fock basis set for an atom in the potential box of fixed radius R_a. However, instead of introducing an infinite potential barrier on the border of the box, we fix the exponential asymptotic behavior of the electron orbitals for $r>R_a$. The exponent corresponds to the asymptotic behavior of the exact many-body wave function for the case when one electron goes to the large distances. For each partial wave the exponent is chosen independently and is taken from an analysis of the experimental atomic spectrum. For $r<R_a$ the orbitals are solutions of the radial Dirac-Fock equations. Having the correct asymptotic behavior of the atomic wave function at large distances allows us to use smaller values of R_a than for an ordinary potential box. This results in a smaller number of orbitals per unit energy interval, i.e., faster convergence of the CI method. Although the advantage of this basis for the calculation of the low-lying states is essential, its shortcoming is a necessity to redefine the basis set for the calculation of the higher states.

The second basis set includes several Dirac-Fock orbitals for the lower valence one-particle states while the other orbitals are obtained from the former by multiplying them by powers of r and orthogonalizing the product to all other orbitals with the same l and j. Similar basis sets have been used in nonrelativistic atomic calculations before (see, for example, [27,28]). When orbitals of this type are used in relativistic calculations, it is necessary to ensure orthogonality to the Dirac orbitals with negative energy (positron states). That can be done by using the kinetic balance condition for the small components of the Dirac bispinors [23].

IV. APPLICATION TO Tl, Tl^+, AND Tl^{++}

We have chosen thallium to test the method because it is the second simplest atom (after cesium) among those used in the ongoing PNC experiments. Thallium has the configura-

TABLE I. Comparison of the parameters of the core in the MBPT calculations of cesium ($1s^2\cdots5p^6$) and thallium ($1s^2\cdots6s^2$) with those of the core of thallium used in this work ($1s^2\cdots5d^{10}$).

	MBPT		CI+MBPT
	Cs [a]	Tl [b]	Tl
rms radius of the last shell	2.2	2.6	1.5
binding energy of the last shell	0.66	0.69	1.07
smallest excitation energy for the dipole transitions	0.53	0.44	0.82
dipole polarizability	17	24	7

[a]References [9,10]. [b]Reference [29].

tion $6s^26p$, and can be treated within MBPT as an atom with one electron above a closed-shell core [29]. However, as we mentioned above, the accuracy of such calculations appears to be lower than for cesium. The main reason for this is the small binding energy and diffuseness of the $6s^2$ shell, which strongly interacts with the $6p$ electron.

Thus, we define the core as $[1s^2\cdots5d^{10}]$, leaving three electrons in the CI space. It is interesting to compare this core with those used in the MBPT calculations of Cs [9,10] and Tl [29]. In Table I several parameters, which are important for the convergence of MBPT, are given for all three cores. Comparison of these parameters indicates that the core used here is likely to provide much better convergence for MBPT than the two others.

There is one interesting feature of the combined method used here. Formally, for the MBPT calculations of Σ the number of valence electrons is not fixed. In Sec. III we showed that Σ can be defined in terms of radial integrals, which correspond to the complete set of diagrams. Using these radial integrals we can calculate Σ for all possible valence configurations, including those which correspond to the ionized atoms. We started with the calculations for neutral thallium and then used the same radial integrals to calculate the ions Tl^+ and Tl^{++}.

For the MBPT part of the problem we use the V^{N-1} approximation which corresponds to the solution of the Dirac-Fock equations for the configuration $1s^2\cdots5d^{10}6s^2$. As was shown in Sec. III, this choice requires calculation of the subtraction diagrams with summations over the two $6s$ electrons in the blocks shown in Fig. 1.

Tables II and III present the contributions of different diagrams to several one-electron and two-electron effective radial integrals. It is seen that subtraction diagrams are quite important for the self-energy but are negligible for screening. Box diagrams significantly reduce screening for the zero multipolarity.

In the last row of Table II, derivatives of the matrix elements of the self-energy operator with respect to the energy are given. For thallium these derivatives are typically of the order of $(1–3)\times10^{-2}$. This means that the dependence of the energy denominators on configuration can contribute significantly to the calculated energy levels (see discussion in Sec. III). We chose the denominators to be correct for the $6s^26p$ configuration. As this configuration constitutes 98% of the ground state, the correction associated with the energy-dependence of Σ is small for the ground state. However, it will not be so small for the excited states. This could be one of the sources of the lower accuracy of our results for the excited states (see also the discussion of the basis set problems below).

TABLE II. The self-energy part of the correlation interaction of the valence electrons with the atomic core (cm^{-1}). The contributions of the mirror diagrams are included. In the last two rows of the table the resultant matrix elements of the operator Σ and its derivative with respect to the energy are given.

Diagram	$D_{6s_{1/2},6s_{1/2}}$	$D_{6p_{1/2},6p_{1/2}}$	$D_{6p_{3/2},6p_{3/2}}$
Fig. 2.1	−23000	−13403	−9777
Fig. 2.2	2848	2081	1456
Fig. 2.3	4522	1704	1110
Fig. 2.4	−1795	−502	−306
Fig. 3.1	6000	2329	1533
Fig. 3.2	1445	547	361
Fig. 3.3	1445	988	760
Fig. 3.4	536	261	164
Fig. 3.5	11	11	17
Fig. 3.6	−11	16	29
Fig. 3.7	3	6	13
$\langle\Sigma\rangle$	−7996	−5962	−4640
$\langle\partial_E\Sigma\rangle$	−0.031	−0.027	−0.023

We also calculated the diagram in Fig. 6 for the two relativistic configurations $6s^26p_{1/2}$ and $6s^26p_{3/2}$. After summing over all permutations, we found that the effective three-particle interaction changes the energy of these states by only $-11\ cm^{-1}$ and $+0.2\ cm^{-1}$, respectively. Therefore, we did not include it in the effective Hamiltonian.

The results of the different approximations for several levels of neutral thallium are given in Table IV. The typical accuracy of the Dirac-Fock method is about 10%. The CI method improves the accuracy for the lower levels by a factor of 2. Note that the two orbital basis sets described above give very close results for the two lowest levels, while for the higher levels there is a growing difference between them. We

TABLE III. The screening of some diagonal Coulomb radial integrals for zero multipolarity $R^0_{a,a,a,a}$ (cm^{-1}). The contributions of the mirror diagrams are included.

Diagram	$a=6s_{1/2}$	$a=6p_{1/2}$	$a=6p_{3/2}$
Coulomb[a]	80051	55425	48322
Fig. 4.1	−3000	−500	−225
Fig. 4.2	−723	−200	−104
Fig. 4.3	−723	−200	−104
Fig. 4.4	270	270	158
Fig. 4.5	270	270	158
Fig. 4.6	−437	−27	−13
Fig. 5.1	−11	−4	−4
Fig. 5.2	−11	−4	−4
Fig. 5.3	6	−3	−3
Fig. 5.4	6	−3	−3
Sum[b]	75698	55024	48178

[a]Radial integral for the unscreened Coulomb interaction.
[b]Radial integral for the screened Coulomb interaction.

TABLE IV. Binding energies for thallium in different approximations in comparison with experiment (cm^{-1}).

Config.	J	HF [a]	CI [b,c]	CI [b,d]	CI + SE [e]	CI + SE + SC [f]	Expt. [30]
$6s^2 6p$	1/2	43827	46865	46855	52152	49507	49264
$6s^2 6p$	3/2	36639	39760	39752	44051	41655	41471
$6s^2 7s$	1/2	21108	21487	21303		22459	22787
$6s^2 7p$	1/2	14276	14526	13835		14726	15104
$6s^2 7p$	3/2	13357	13582	12912		13726	14103
$6s^2 6d$	3/2	12218		7684		12940	13146
$6s^2 6d$	5/2	12167		7686		12867	13064

[a]One-electron relativistic Hartree-Fock approximation.

[b]Ordinary configuration interaction method. No core excitations have been taken into account.

[c]Basis set No. 1.

[d]Basis set No. 2.

[e]Configuration interaction with self-energy part of correlations between valence and core electrons included (diagrams in Figs. 2 and 3).

[f]Configuration interaction with both self-energy and screening of the valence-valence interaction included.

have already pointed out that the first basis set is actually linked to the certain atomic states by the choice of the asymptotic behavior. So, it is not surprising that for the excited states the results obtained with the second basis set are somewhat better. Still, even for the second basis set we were able to saturate the CI for the first two levels only.

Table IV shows that the addition of the self-energy corrections to the effective Hamiltonian results in a significant overestimation of the binding energy. A radical improvement of the accuracy is achieved only when screening is also taken into account. Our final accuracy for the two lower levels is better than 0.5%, which is an order of magnitude improvement in comparison with the conventional CI method. For the higher levels the CI has not been saturated, so they cannot be used as a test of the method, but improvement of the results is clearly seen.

In Table V the results of the calculations for the positive ions are given. Again, there is about an order of magnitude improvement of the accuracy in comparison with the CI method. Note that for Tl^{2+} there is only one valence electron, and thus only the self-energy corrections are important.

V. CONCLUSION

The combination of the CI and MBPT methods presented in this paper is actually a new method which retains the advantages of both of the methods that it is based on. First, the many-body problem for the valence electrons is solved accurately, assuming that the convergence regarding the basis set used has been achieved. Second, the core-valence and core-core correlations which are important but small enough to be treated accurately by means of the MBPT are also included. The implementation of the method has a very convenient form. The second-order diagrams are calculated in the single-electron basis and do not depend on the configuration of the valence electrons. Thus, their inclusion is reduced to the redefinition of the one- and two-electron matrix elements of the ordinary CI Hamiltonian. The CI method itself remains almost untouched. A similar approach is feasible for the calculation of transition amplitudes. This is the direction of our further efforts.

The results obtained for the energy levels of Tl, Tl^+, and Tl^{2+} show that the method has great potential. From our point of view it presents a powerful alternative to the existing methods of high precision relativistic calculations for many-electron atoms.

ACKNOWLEDGMENTS

The authors are grateful to G. Gribakin, M. Kuchiev, and O. Sushkov for many extremely helpful discussions. We thank S. Porsev for reading the manuscript. This work was

TABLE V. Calculated binding energies for Tl^+ and Tl^{++} in comparison with experiment (cm^{-1}).

Ion	Config.	J	CI	CI + SE + SC	Expt. [30,31]
Tl^+	$6s^2$	0	156114	165379	164765
	$6s6p$	0	112380	115061	115314
	$6s6p$	1	109122	112271	112372
	$6s6p$	2	100295	102586	103040
	$6s6p$	1	81875	90726	89105
	$6s7s$	1	55957	58429	59540
	$6s7s$	0	53653	55537	56769
Tl^{++}	$6s$	1/2	232680	240681	240770
	$6p$	1/2	169981	177188	176614
	$6p$	3/2	155766	162264	161800
	$7s$	1/2	91702	100398	101561

supported in part by the Australian Research Council, by Grant No. R3Q300 from the International Science Foundation and the Russian Government, by Grant No. 95-02-03701-A from the Russian Foundation for Basic Research, and by the National Science Foundation through a grant for the Institute for Theoretical Atomic and Molecular Physics at Harvard University and Smithsonian Astrophysical Observatory. One of us (M.K.) is also grateful to UNSW for hospitality; V.F. is grateful to ITAMP for hospitality.

APPENDIX: ANALYTICAL EXPRESSIONS FOR THE SECOND-ORDER DIAGRAMS

In this appendix we give expressions for the diagrams in Figs. 2–5. We are not writing sums explicitly: it is assumed that summation takes place over all indices which correspond to internal lines, as well as over the multipolarities of the Coulomb interactions, k_1 and k_2. The following conventions for the indices are used: a,b,c, and d correspond to the external lines; $1\leqslant m,n\leqslant N_{\rm core}$; $N_{\rm core}+1\leqslant i,j\leqslant N_{\rm DF}$ and $N_{\rm core}+1\leqslant\alpha,\beta$. We also assume that the first Coulomb interaction (k_1) is always connected to the line a. In the expressions given below, all summations over the projections of the angular momenta have already been made. In this Appendix we use the standard MBPT definition of the energy denominators. For the discussion of the possible modifications of this definition see Sec. III.

The matrix element of the Coulomb interaction for the multipolarity k is equal to

$$\langle c,d|V^k_q|a,b\rangle=(-1)^{m_c+m_b+1}\delta_p\sqrt{(2j_a+1)(2j_b+1)(2j_c+1)(2j_d+1)}\begin{pmatrix} j_c & j_a & k\\ -m_c & m_a & q\end{pmatrix}\begin{pmatrix} j_b & j_d & k\\ -m_b & m_d & q\end{pmatrix}$$
$$\times\begin{pmatrix} j_c & j_a & k\\ 1/2 & -1/2 & 0\end{pmatrix}\begin{pmatrix} j_b & j_d & k\\ 1/2 & -1/2 & 0\end{pmatrix}R^k_{a,b,c,d}, \tag{A1}$$

where $R^k_{a,b,c,d}$ is the radial integral and δ_p accounts for the parity selection rule:

$$\delta_p=\xi(l_a+l_c+k)\xi(l_b+l_d+k), \tag{A2}$$

$$\xi(n)=\begin{cases}1 & \text{if } n \text{ is even,}\\ 0 & \text{if } n \text{ is odd.}\end{cases} \tag{A3}$$

Let us start with the contributions to the self-energy matrix elements from the four main diagrams (Fig. 2).

$$D_{a,b}\ (\text{Fig. } 2.1)=\delta_{k_1,k_2}\delta_{j_a,j_b}\delta_{m_a,m_b}\frac{(2j_\alpha+1)(2j_\beta+1)(2j_n+1)}{2k_1+1}\begin{pmatrix} j_a & j_\beta & k_1\\ 1/2 & -1/2 & 0\end{pmatrix}^2\begin{pmatrix} j_\alpha & j_n & k_1\\ 1/2 & -1/2 & 0\end{pmatrix}^2\frac{R^{k_1}_{a,n,\beta,\alpha}R^{k_1}_{b,n,\beta,\alpha}}{\epsilon_a+\epsilon_n-\epsilon_\alpha-\epsilon_\beta}, \tag{A4}$$

$$D_{a,b}\ (\text{Fig. } 2.2)=(-1)^{k_1+k_2}\delta_{j_a,j_b}\delta_{m_a,m_b}(2j_\alpha+1)(2j_\beta+1)(2j_n+1)\begin{Bmatrix} j_a & j_\alpha & k_2\\ j_n & j_\beta & k_1\end{Bmatrix}\begin{pmatrix} j_a & j_\beta & k_1\\ 1/2 & -1/2 & 0\end{pmatrix}\begin{pmatrix} j_\alpha & j_n & k_1\\ 1/2 & -1/2 & 0\end{pmatrix}$$
$$\times\begin{pmatrix} j_a & j_\alpha & k_2\\ 1/2 & -1/2 & 0\end{pmatrix}\begin{pmatrix} j_\beta & j_n & k_2\\ 1/2 & -1/2 & 0\end{pmatrix}\frac{R^{k_1}_{a,n,\beta,\alpha}R^{k_2}_{b,n,\alpha,\beta}}{\epsilon_a+\epsilon_n-\epsilon_\alpha-\epsilon_\beta}, \tag{A5}$$

$$D_{a,b}\ (\text{Fig. } 2.3)=-\delta_{k_1,k_2}\delta_{j_a,j_b}\delta_{m_a,m_b}\frac{(2j_\alpha+1)(2j_m+1)(2j_n+1)}{2k_1+1}$$
$$\times\begin{pmatrix} j_a & j_m & k_1\\ 1/2 & -1/2 & 0\end{pmatrix}^2\begin{pmatrix} j_n & j_\alpha & k_1\\ 1/2 & -1/2 & 0\end{pmatrix}^2\frac{R^{k_1}_{a,n,m,\alpha}R^{k_1}_{b,n,m,\alpha}}{\epsilon_m+\epsilon_n-\epsilon_\alpha-\epsilon_b}, \tag{A6}$$

$$D_{a,b}\ (\text{Fig. } 2.4)=(-1)^{k_1+k_2+1}\delta_{j_a,j_b}\delta_{m_a,m_b}(2j_\alpha+1)(2j_m+1)(2j_n+1)\begin{Bmatrix} j_a & j_m & k_2\\ j_\alpha & j_n & k_1\end{Bmatrix}\begin{pmatrix} j_a & j_m & k_1\\ 1/2 & -1/2 & 0\end{pmatrix}$$
$$\times\begin{pmatrix} j_n & j_\alpha & k_1\\ 1/2 & -1/2 & 0\end{pmatrix}\begin{pmatrix} j_a & j_n & k_2\\ 1/2 & -1/2 & 0\end{pmatrix}\begin{pmatrix} j_m & j_\alpha & k_2\\ 1/2 & -1/2 & 0\end{pmatrix}\frac{R^{k_1}_{a,\alpha,m,n}R^{k_2}_{b,\alpha,n,m}}{\epsilon_m+\epsilon_n-\epsilon_\alpha-\epsilon_\beta}. \tag{A7}$$

In Fig. 3 only the significantly different subtraction diagrams are shown. Each of the asymmetric diagrams (1–4 and 6) represents a pair of two diagrams related by reflection. Below we only give the expressions for those diagrams shown in Fig. 3.

$$D_{a,b}\ (\text{Fig. } 3.1) = -\delta_{j_a,j_b}\delta_{m_a,m_b}\delta_{k_1,0}\delta_{k_2,0}\delta_{j_n,j_\alpha}(2j_i+1)(2j_n+1)\frac{R^0_{a,\alpha,b,n}R^0_{i,n,i,\alpha}}{\epsilon_n-\epsilon_\alpha}, \tag{A8}$$

$$D_{a,b}\ (\text{Fig. } 3.2) = \delta_{j_a,j_b}\delta_{m_a,m_b}\delta_{k_1,0}\delta_{j_n,j_\alpha}(2j_i+1)(2j_n+1)\begin{pmatrix} j_n & j_i & k_2 \\ 1/2 & -1/2 & 0 \end{pmatrix}^2 \frac{R^0_{a,\alpha,b,n}R^{k_2}_{n,i,i,\alpha}}{\epsilon_n-\epsilon_\alpha}, \tag{A9}$$

$$D_{a,b}\ (\text{Fig. } 3.3) = \delta_{j_a,j_b}\delta_{m_a,m_b}\delta_{k_2,0}\delta_{j_n,j_\alpha}(2j_i+1)(2j_n+1)\begin{pmatrix} j_a & j_n & k_1 \\ 1/2 & -1/2 & 0 \end{pmatrix}^2 \frac{R^{k_1}_{a,\alpha,n,b}R^0_{\alpha,i,n,i}}{\epsilon_n-\epsilon_\alpha}, \tag{A10}$$

$$D_{a,b}\ (\text{Fig. } 3.4) = -\delta_{j_a,j_b}\delta_{m_a,m_b}\delta_{j_n,j_\alpha}(2j_i+1)(2j_n+1)\begin{pmatrix} j_a & j_n & k_1 \\ 1/2 & -1/2 & 0 \end{pmatrix}^2\begin{pmatrix} j_n & j_i & k_2 \\ 1/2 & -1/2 & 0 \end{pmatrix}^2 \frac{R^{k_1}_{a,\alpha,n,b}R^{k_2}_{\alpha,i,i,n}}{\epsilon_n-\epsilon_\alpha}, \tag{A11}$$

$$D_{a,b}\ (\text{Fig. } 3.5) = -\delta_{j_a,j_b}\delta_{m_a,m_b}\delta_{k_1,0}\delta_{k_2,0}\delta_{j_n,j_a}(2j_i+1)(2j_j+1)\frac{R^0_{a,j,n,j}R^0_{b,i,n,i}}{\epsilon_n-\epsilon_b}, \tag{A12}$$

$$D_{a,b}\ (\text{Fig. } 3.6) = \delta_{j_a,j_b}\delta_{m_a,m_b}\delta_{k_1,0}\delta_{j_n,j_a}(2j_i+1)(2j_j+1)\begin{pmatrix} j_a & j_i & k_2 \\ 1/2 & -1/2 & 0 \end{pmatrix}^2 \frac{R^0_{a,j,n,j}R^{k_2}_{b,n,i,i}}{\epsilon_n-\epsilon_b}, \tag{A13}$$

$$D_{a,b}\ (\text{Fig. } 3.7) = -\delta_{j_a,j_b}\delta_{m_a,m_b}\delta_{j_n,j_a}(2j_i+1)(2j_j+1)\begin{pmatrix} j_a & j_j & k_1 \\ 1/2 & -1/2 & 0 \end{pmatrix}^2\begin{pmatrix} j_a & j_i & k_2 \\ 1/2 & -1/2 & 0 \end{pmatrix}^2 \frac{R^{k_1}_{a,n,j,j}R^{k_2}_{b,n,i,i}}{\epsilon_n-\epsilon_b}. \tag{A14}$$

The diagrams in Figs. 4 and 5 correspond to the corrections to the Coulomb interaction between the valence electrons. Thus, it is convenient to separate the angular and radial parts as in Eq. (A1). Below we give the expressions for the effective radial integrals associated with each diagram. Note that the standard parity selection rule [which is accounted for by the factor δ_p (31)] holds for the diagrams in Figs. 4.1 – 4.3, as well as for all subtraction diagrams in Fig. 5, but not for the box diagrams in Figs. 4.4 – 4.6.

The effective radial integrals for the screening diagrams in Fig. 4 are

$$R^k_{a,c,b,d}\ (\text{Fig. } 4.1) = \delta_{k_1,k}\delta_{k_2,k}\delta_p\frac{(2j_n+1)(2j_\alpha+1)}{2k+1}\begin{pmatrix} j_\alpha & j_n & k \\ 1/2 & -1/2 & 0 \end{pmatrix}^2 \frac{R^k_{a,\alpha,b,n}R^k_{c,\alpha,d,n}}{\epsilon_c+\epsilon_n-\epsilon_d-\epsilon_\alpha}, \tag{A15}$$

$$R^k_{a,c,b,d}\ (\text{Fig. } 4.2) = (-1)^{k_1+k}\delta_{k_2,k}\delta_p(2j_n+1)(2j_\alpha+1)\begin{Bmatrix} j_a & j_b & k \\ j_\alpha & j_n & k_1 \end{Bmatrix}\begin{pmatrix} j_b & j_\alpha & k_1 \\ 1/2 & -1/2 & 0 \end{pmatrix}\begin{pmatrix} j_a & j_n & k_1 \\ 1/2 & -1/2 & 0 \end{pmatrix}$$
$$\times\begin{pmatrix} j_\alpha & j_n & k \\ 1/2 & -1/2 & 0 \end{pmatrix}\times\begin{pmatrix} j_b & j_a & k \\ 1/2 & -1/2 & 0 \end{pmatrix}^{-1}\frac{R^{k_1}_{a,\alpha,n,b}R^k_{c,\alpha,d,n}}{\epsilon_c+\epsilon_n-\epsilon_d-\epsilon_\alpha}, \tag{A16}$$

$$R^k_{a,c,b,d}\ (\text{Fig. } 4.3) = (-1)^{k+k_2}\delta_{k_1,k}\delta_p(2j_n+1)(2j_\alpha+1)\begin{Bmatrix} j_c & j_d & k_2 \\ j_n & j_\alpha & k \end{Bmatrix}\begin{pmatrix} j_c & j_\alpha & k_2 \\ 1/2 & -1/2 & 0 \end{pmatrix}\begin{pmatrix} j_d & j_n & k_2 \\ 1/2 & -1/2 & 0 \end{pmatrix}$$
$$\times\begin{pmatrix} j_n & j_\alpha & k \\ 1/2 & -1/2 & 0 \end{pmatrix}\begin{pmatrix} j_d & j_c & k \\ 1/2 & -1/2 & 0 \end{pmatrix}^{-1}\frac{R^k_{a,\alpha,b,n}R^{k_2}_{d,\alpha,n,c}}{\epsilon_c+\epsilon_n-\epsilon_d-\epsilon_\alpha}, \tag{A17}$$

$$R^k_{a,c,b,d}\,(\text{Fig. 4.4}) = (-1)^{j_a+j_b+j_c+j_d+j_\alpha+j_n}(2j_n+1)(2j_\alpha+1)(2k+1)\begin{Bmatrix} j_b & j_a & k \\ k_1 & k_2 & j_n \end{Bmatrix}\begin{Bmatrix} j_c & j_d & k \\ k_1 & k_2 & j_\alpha \end{Bmatrix}\begin{pmatrix} j_a & j_n & k_1 \\ 1/2 & -1/2 & 0 \end{pmatrix}$$
$$\times\begin{pmatrix} j_d & j_\alpha & k_1 \\ 1/2 & -1/2 & 0 \end{pmatrix}\begin{pmatrix} j_b & j_n & k_2 \\ 1/2 & -1/2 & 0 \end{pmatrix}\begin{pmatrix} j_c & j_\alpha & k_2 \\ 1/2 & -1/2 & 0 \end{pmatrix}\begin{pmatrix} j_b & j_a & k \\ 1/2 & -1/2 & 0 \end{pmatrix}^{-1}$$
$$\times\begin{pmatrix} j_c & j_d & k \\ 1/2 & -1/2 & 0 \end{pmatrix}^{-1}\frac{R^{k_1}_{a,\alpha,n,d}R^{k_2}_{b,\alpha,n,c}}{\epsilon_c+\epsilon_n-\epsilon_b-\epsilon_\alpha}, \tag{A18}$$

$$R^k_{a,c,b,d}\,(\text{Fig. 4.5}) = (-1)^{j_a+j_b+j_c+j_d+j_\alpha+j_n}(2j_n+1)(2j_\alpha+1)(2k+1)\begin{Bmatrix} j_b & j_a & k \\ k_1 & k_2 & j_\alpha \end{Bmatrix}\begin{Bmatrix} j_c & j_d & k \\ k_1 & k_2 & j_n \end{Bmatrix}\begin{pmatrix} j_a & j_\alpha & k_1 \\ 1/2 & -1/2 & 0 \end{pmatrix}$$
$$\times\begin{pmatrix} j_d & j_n & k_1 \\ 1/2 & -1/2 & 0 \end{pmatrix}\begin{pmatrix} j_b & j_\alpha & k_2 \\ 1/2 & -1/2 & 0 \end{pmatrix}\begin{pmatrix} j_c & j_n & k_2 \\ 1/2 & -1/2 & 0 \end{pmatrix}\begin{pmatrix} j_b & j_a & k \\ 1/2 & -1/2 & 0 \end{pmatrix}^{-1}$$
$$\times\begin{pmatrix} j_c & j_d & k \\ 1/2 & -1/2 & 0 \end{pmatrix}^{-1}\frac{R^{k_1}_{a,n,\alpha,d}R^{k_2}_{b,n,\alpha,c}}{\epsilon_c+\epsilon_n-\epsilon_d-\epsilon_\alpha}, \tag{A19}$$

$$R^k_{a,c,b,d}\,(\text{Fig. 4.6}) = (-1)^{j_a+j_b+j_c+j_d+j_m+j_n+k_1+k_2+k+1}(2j_m+1)(2j_n+1)(2k+1)\begin{Bmatrix} j_b & j_a & k \\ k_1 & k_2 & j_m \end{Bmatrix}\begin{Bmatrix} j_c & j_d & k \\ k_2 & k_1 & j_n \end{Bmatrix}$$
$$\times\begin{pmatrix} j_m & j_a & k_1 \\ 1/2 & -1/2 & 0 \end{pmatrix}\begin{pmatrix} j_c & j_n & k_1 \\ 1/2 & -1/2 & 0 \end{pmatrix}\begin{pmatrix} j_b & j_m & k_2 \\ 1/2 & -1/2 & 0 \end{pmatrix}\begin{pmatrix} j_n & j_d & k_2 \\ 1/2 & -1/2 & 0 \end{pmatrix}\begin{pmatrix} j_b & j_a & k \\ 1/2 & -1/2 & 0 \end{pmatrix}^{-1}$$
$$\times\begin{pmatrix} j_c & j_d & k \\ 1/2 & -1/2 & 0 \end{pmatrix}^{-1}\frac{R^{k_1}_{a,c,m,n}R^{k_2}_{b,d,m,n}}{\epsilon_m+\epsilon_n-\epsilon_b-\epsilon_d}. \tag{A20}$$

Effective radial integrals for the subtraction diagrams (Fig. 5) are

$$R^k_{a,c,b,d}\,(\text{Fig. 5.1}) = \delta_{j_a,j_n}\delta_{k_1,0}\delta_{k_2,k}\delta_p(2j_i+1)\frac{R^0_{a,i,n,i}R^k_{b,d,n,c}}{\epsilon_c+\epsilon_n-\epsilon_b-\epsilon_d}, \tag{A21}$$

$$R^k_{a,c,b,d}\,(\text{Fig. 5.2}) = \delta_{j_d,j_n}\delta_{k_2,0}\delta_{k_1,k}\delta_p(2j_i+1)\frac{R^k_{a,c,b,n}R^0_{d,i,n,i}}{\epsilon_n-\epsilon_d}, \tag{A22}$$

$$R^k_{a,c,b,d}\,(\text{Fig. 5.3}) = -\delta_{j_a,j_n}\delta_{k_2,k}\delta_p(2j_i+1)\begin{pmatrix} j_a & j_i & k_1 \\ 1/2 & -1/2 & 0 \end{pmatrix}^2\frac{R^{k_1}_{a,i,i,n}R^k_{b,d,n,c}}{\epsilon_c+\epsilon_n-\epsilon_b-\epsilon_d}, \tag{A23}$$

$$R^k_{a,c,b,d}\,(\text{Fig. 5.4}) = -\delta_{j_d,j_n}\delta_{k_1,k}\delta_p(2j_i+1)\begin{pmatrix} j_d & j_i & k_2 \\ 1/2 & -1/2 & 0 \end{pmatrix}^2\frac{R^k_{a,c,b,n}R^{k_2}_{d,i,i,n}}{\epsilon_n-\epsilon_d}. \tag{A24}$$

[1] I. B. Khriplovich, *Parity Non-Conservation in Atomic Phenomena* (Gordon and Breach, New York, 1991).

[2] A.-M. Mårtensson-Pendrill, in *Methods in Computational Chemistry, Vol. 5: Atomic and Molecular Properties*, edited by S. Wilson (Plenum Press, New York, 1992).

[3] S. M. Barr, Int. J. Mod. Phys. A **8**, 209 (1993).

[4] M. G. Kozlov and L. N. Labzowsky, J. Phys. B **28**, 1933 (1995).

[5] S. L. Gilbert, M. C. Noecker, R. N. Watts, and C. E. Wieman, Phys. Rev. Lett. **55**, 2680 (1985); M. C. Noecker, B. P. Masterson, C. E. Wieman, *ibid.* **61**, 310 (1988).

[6] D. M. Meekhof, P. Vetter, P. K. Majumder, S. K. Lamoreaux,

and E. N. Fortson, Phys. Rev. Lett. **71**, 3442 (1993).
[7] N. H. Edwards, S. J. Phipp, P. E. G. Baird, and S. Nakayama, Phys. Rev. Lett. **74**, 2654 (1995); P. A. Vetter, D. M. Meekhof, P. K. Majumder, S. K. Lamoreaux, and E. N. Fortson, *ibid.* **74**, 2658 (1995).
[8] M. J. D. Macpherson, K. P. Zetie, R. B. Warrington, D. N. Stacey, and J. P. Hoare, Phys. Rev. Lett. **67**, 2784 (1991).
[9] V. A. Dzuba, V. V. Flambaum, and O. P. Sushkov, Phys. Lett. A **141**, 147 (1989).
[10] S. A. Blundell, W. R. Johnson, and J. Sapirstein, Phys. Rev. Lett. **65**, 1411 (1990).
[11] V. A. Dzuba, V. V. Flambaum, and O. P. Sushkov, Phys. Rev. A **51**, 3454 (1995).
[12] I. Lindgren and J. Morrison, *Atomic Many-Body Theory*, 2nd ed. (Springer-Verlag, Berlin, 1985).
[13] V. A. Dzuba, V. V. Flambaum, P. G. Silvestrov, and O. P. Sushkov, J. Phys. B **20**, 1399 (1987).
[14] V. A. Dzuba, V. V. Flambaum, and O. P. Sushkov, Phys. Lett. A **140**, 493 (1989).
[15] V. A. Dzuba, V. V. Flambaum, and O. P. Sushkov, Phys. Lett. A **142**, 373 (1989).
[16] V. A. Dzuba, V. V. Flambaum, P. G. Silvestrov, and O. P. Sushkov, Phys. Lett. A **131**, 461 (1988).
[17] A. A. Blundell, W. R. Johnson, and J. Sapirstein, Phys. Rev. A **43**, 3407 (1991).
[18] E. Ilybaev and U. Kaldor, Phys. Rev. A **47**, 137 (1993); E. Elian, U. Kaldor, and Y. Ishikawa, Phys. Rev. A **49**, 1724 (1994); **50**, 1121 (1994); **51**, 225 (1995).
[19] I. P. Grant and H. M. Quiney, Adv. At. Mol. Phys. **23**, 37 (1988).
[20] P. Jonsson, C. Froese Fischer, Phys. Rev. A **50**, 3080 (1994); A. Aboussaid, M. R. Godefroid, P. Jonsson, and C. Froese Fischer, *ibid.* **51**, 2031 (1995); C. Froese Fischer, J. E. Hansen, and H. W. van den Hart, *ibid.* **51**, 1999 (1995); J. E. Sienkiewicz, S. Fritzsche, and I. P. Grant, J. Phys. B **28**, L633 (1995).
[21] V. A. Dzuba, V. V. Flambaum, and M. G. Kozlov, Phys. Rev. A **50**, 3812 (1994).
[22] S. G. Porsev, Yu. G. Rakhlina, and M. G. Kozlov, Pis'ma Zh. Éksp. Teor. Fiz. **61**, 449 (1995) [JETP Lett. **61**, 459 (1995)].
[23] M. G. Kozlov and S. G. Porsev, Petersburg Nuclear Physics Institute Report No. TH-4-1995 2031, 1995 (unpublished); M. G. Kozlov, S. G. Porsev, and V. V. Flambaum, J. Phys. B **29**, 689 (1996).
[24] V. A. Dzuba, V. V. Flambaum, and M. G. Kozlov, Pis'ma Zh. Éksp. Teor. Fiz. **63**, 844 (1996) [JETP Lett. **63**, 882 (1996)].
[25] V. A. Dzuba, V. V. Flambaum, and O. P. Sushkov, J. Phys. B **16**, 715 (1983).
[26] I. Lindgren, J. Phys. B **7**, 2441 (1974).
[27] P. O. Bogdanovich, thesis, 1988 (unpublished).
[28] E. L. Shirley and R. M. Martin, Phys. Rev. B **47**, 15 404 (1993).
[29] V. A. Dzuba, V. V. Flambaum, P. G. Silvestrov, and O. P. Sushkov, J. Phys. B **20**, 3297 (1987).
[30] C. E. Moore, *Atomic Energy Levels*, Natl. Bur. Stand. (U.S.) Circ. No. 467 (U.S. GPO, Washington, D.C., 1958).
[31] A. A. Radzig and B. M. Smirnov, *Parameters of Atoms and Atomic Ions* (Energoatomizdat, Moscow, 1986) (in Russian).